Tellus (1989), *41A*, 209–221

Zonal wave number 2 baroclinic outbreak episodes in winter

By HEINZ-DIETER SCHILLING, *Meteorological Institute, University of Bonn, Auf dem Hügel 20, D5300 Bonn 1, FRG*

(Manuscript received 18 March 1987; in final form 29 July 1988)

ABSTRACT

Long-lasting episodes, so-called baroclinic outbreaks (BO), with extra-ordinary baroclinic conversions favouring one ultralong wave with zonal wavenumber m were studied in a previous paper (Schilling, 1988). This paper is concentrated on $m = 2$ winter BO's with durations of more than 7 days. In addition, almost hemispherically-averaged energy parameters ($10°\text{N} \leqslant \phi \leqslant 90°\text{N}$) and a two-dimensional spectral representation ($\tilde{n}$ is the meridional mode index) are used. From 10 years (1967–1976) of data, we find 15 ultra-persistent winter cases, but only 11 are considered for further investigation, since 4 episodes fail to show sufficient growth of kinetic energy of $m = 2$ (K_2) despite large input $C(A_z A_2)$. During $m = 2$ BO's in winter, the meridional mode $\tilde{n} = 2$ (one node between southern boundary at 10°N and pole) exhibits large amplification and K_2 concentrates dramatically in precisely this mode. Mainly, the available potential energy of the super-rotational mode of the zonal mean vertical wind shear supplies that energy inflow. During the first stages of $m = 2$ BO's, the kinetic energy and baroclinic activity of synoptic waves ($m = 5$–8) appear to be significantly suppressed. An unusual distribution of modal eddy kinetic energy in 500 mb results so that approximately 25–30% of it is concentrated in only one wave mode ($m = 2$, $\tilde{n} = 2$).

1. Introduction

In the last few years, increasing interest in studies on ensembles of similar events by means of energetics analysis is perceivable. For instance, this approach was adopted for the analysis of cold air outbreaks (Kung and Masters, 1983) or for the blocking problem (see Hansen and Sutera, 1984; Schilling, 1986; Hansen and Chen, 1982; Fischer, 1984). Generally, the interpretation of the events fails to provide conclusive results, as long as they are defined synoptically. The reason being that synoptic patterns show the integral effect of different cooperating processes rather than a well-defined mechanism. A similar reasoning is valid for defining events by amplification episodes (Tsay and Kao, 1978a, b; Itoh, 1983; Hansen, 1986). Although these studies have contributed to our understanding of amplification episodes, they also illustrate how complicated the energy input pattern will often be (Itoh, 1983).

We can only hope to draw definite conclusions for an ensemble of events which is more or less homogeneous by definition. In the companion study (Schilling, 1988, hereafter referred to as S88), an improvement is achieved by defining episodes by extraordinarily strong developments of a single energy conversion. This conversion should represent a definite process. The episodes are simplified by definition, because certain restrictions are imposed on their energetic structure, including the specification of source and target of the energy flow.

Daily records of the baroclinic conversions $C(A_z A_m)$ for $m = 2$, 3 (averaged over the troposphere and latitudes north of 40°N) reveal that persistent episodes of large baroclinic input from the zonal mean are more frequent than classical linear theories would have predicted (e.g., Hansen, 1986; Schilling, 1986, 1987). This observation motivates the analysis of the transient part of $C(A_z A_m)$ in terms of the above-mentioned concept, leading to the definition of BO events.

Statistical properties of such events were discussed in some detail in S88 with emphasis on ultralong wave BO episodes. Particularly, it was found that only a few predominant processes cooperate or compete in a simple way to form the BO event in the case of $m = 2$. Above all, the predominant energy flux $A_z \rightarrow A_2 \rightarrow K_2$ developed well above-normal values, thus illustrating the completely nonlinear character of the baroclinic activity in persistent cases. The second conversion $C(A_2 K_2)$ showed obvious similarity to the abnormal development of $C(A_z A_2)$ during the majority of long lasting $m = 2$ BO's [for definitions see eqs. (4), (5), (6)]. Therefore, BO events exhibit new features in addition to the classical picture on ultralong wave dynamics.

In order to enhance the homogeneity of the adopted set of BO events, this study only concentrates on persistent BO events belonging to the ultralong wave $m = 2$ in winters (October–February). On this basis, we intend to study the following problems:

(a) Are there leading triad interactions which dominate the driving of the BO mechanism? Technically, this question leads to a two-dimensional spectral decomposition of the flow fields. Fortunately, interesting spectral distributions of leading energy parameters [e.g., K_2, $C(A_z A_2)$, $C(A_2 K_2)$] among the participating wave modes are to be seen. The spectral results are presented by using composite averages. Both techniques are novel in the study of BO's.

(b) Are the results on BO characteristics only valid for the northern belt or not? Therefore, the averaging domain was extended by shifting the southern boundary from 40° N to 15° N.

(c) Is the observation of decreasing baroclinic activity and kinetic energy of synoptic scales during amplification events of ultralong waves (e.g., S88 and Hansen, 1986) representative or not?

(d) According to the findings of S88, nonlinear wave–wave interactions tend to support the ultralong wave's amplification in persistent cases. Is this an accidental or systematic feature of BO dynamics?

In Section 3, we repeat the definition of BO events and describe our case selection rules, appropriate for the composite technique. In Section 4, we extract a composite picture of the energetics of $m = 2$ BO events of long duration.

2. Data

2.1. Evaluation scheme

We use the same data-base and evaluation procedure as in S88. In order to minimize redundancy, we only compile most important characteristics of our data and of its handling (refer to S88 for further details).

Daily northern hemisphere geopotential height data from the German Weather Service (DWD) was used. The data is available at 1000 mb, 500 mb and 300 mb on a λ, ϕ-grid from $\phi = 15°$ N to $\phi = 85°$ N with increments $\Delta\lambda \times \Delta\phi = 10° \times 5°$ for the years 1967–1976. We added two other latitudes, $\phi_0 = 10°$ N and $\phi_{16} = \phi_e = 90°$ N where the deviations from the zonal mean are set to zero [refer to eq. (9a)]. Each height field Z was decomposed in zonal Fourier-components of zonal wavenumber m and the resulting components of the fields of Φ or streamfunction Ψ were labelled by an index m (e.g., Φ_m), except for $m = 0$. Since we identify the $m = 0$ field component with the zonal mean, it is marked by an overbar (e.g., $\overline{\Phi}$).

The data was evaluated by utilizing a three level quasi-geostrophic model with the streamfunction Ψ on each level being computed via the familiar linear balance equation:

$$\nabla \cdot (f(\phi) \nabla \Psi) = \nabla^2 \Phi. \tag{1}$$

The 3 height fields form two thickness fields $\Delta\Phi = h$, representing the model temperatures. Furthermore, we assume the static stability to be dependent on time only:

$$\sigma_0(t) = [-(1/\rho)\, \partial \ln \theta / \partial p]_{\phi_A}^{85°}. \tag{2}$$

The symbol $[\ ]_{\phi_A}^{\phi_B}$ denotes an average over the latitude band $\phi_A \leqslant \phi \leqslant \phi_B$ and the depth of the troposphere:

$$[Y]_{\phi_A}^{\phi_B} = \sum_{j=1}^{J} (\Delta p_j / p_B) \left(\sum_{k=A}^{B} \overline{Y}(\phi_k) \times \cos\phi_k \Big/ \sum_{k=A}^{B} \cos\phi_k \right) \tag{3}$$

(with $J = 2$ for baroclinic and $J = 3$ for barotropic expressions). We adopt $\phi_A = 40°$ N for the narrow belt and $\phi_A = 10°$ N for nearly hemispheric averages. For further definitions see Appendix A.

The energy reservoirs and conversions relevant for this study are listed below:

(i) the kinetic energy of wave m:

$$K_m = (p_B/g)\left[\frac{1}{2}\left\{\frac{1}{a\cos\phi}\frac{\partial\Psi_m}{\partial\lambda}\right\}^2 + \frac{1}{2}\left\{\frac{\partial\Psi_m}{a\,\partial\phi}\right\}^2\right]_{\phi_A}^{85°}; \quad (4)$$

(ii) conversion of available potential energy (APE) between the zonal mean and zonal wave m:

$$C(A_z A_m) = -(p_B/g\sigma_0)\left[\frac{h_m}{\Delta p_j^2}\{J(\Psi', \bar{h})|_m + J(\bar{\Psi}, h')|_m\}\right]_{\phi_A}^{85°}; \quad (5)$$

(iii) baroclinic conversion between APE and kinetic energy of wave m:

$$C(A_m K_m) = (p_B/g)[f_0 \cdot \omega_m \cdot \partial\Psi_m/\partial p]_{\phi_A}^{85°}. \quad (6)$$

The algorithm for computing the ω_m-field and the problems with these estimates were discussed in S88. The parameter $C(A_z A_m)$ represents the overall baroclinic energy input for the total wave m energy and is therefore taken as a parameter for wave m baroclinic activity. For instance, if the input $C(A_z A_m)$ is large and K_m grows fast at the same time we consider wave m being baroclinically active.

There are two other energy conversions we will refer to in the remainder:

(iv) nonlinear wave–wave interaction with scales $m > 5$ as participants, related to the kinetic energy,

$$BTPLS_m = (p_B/g)[\Psi_m J(\Psi_{1\text{-}5}, \nabla^2\Psi_{6\text{-}12})|_m + \Psi_m J(\Psi_{6\text{-}12}, \nabla^2\Psi')|_m]_{15°}^{85°}; \quad (7)$$

(v) nonlinear wave–wave-interaction within the wavegroup $1 \leqslant m \leqslant 5$, related to the kinetic energy,

$$BTPLL_m = (p_B/g)[\Psi_m J(\Psi_{1\text{-}5}, \nabla^2\Psi_{1\text{-}5})|_{m\neq 0}]_{15°}^{85°}. \quad (8)$$

2.2. *Meridional decomposition of fields*

It was found to be practical to decompose each Z-field Fourier component $a_m + ib_m$ into meridional modes, utilizing eigenvectors P_n^m of the Laplacian

$$\nabla^2 Y_n^m = -\lambda_{mn}^2 Y_n^m, \quad Y_n^m = P_n^m \exp(im\lambda); \quad (P_n^m \text{ real}), \quad (9a)$$

subject to the boundary conditions

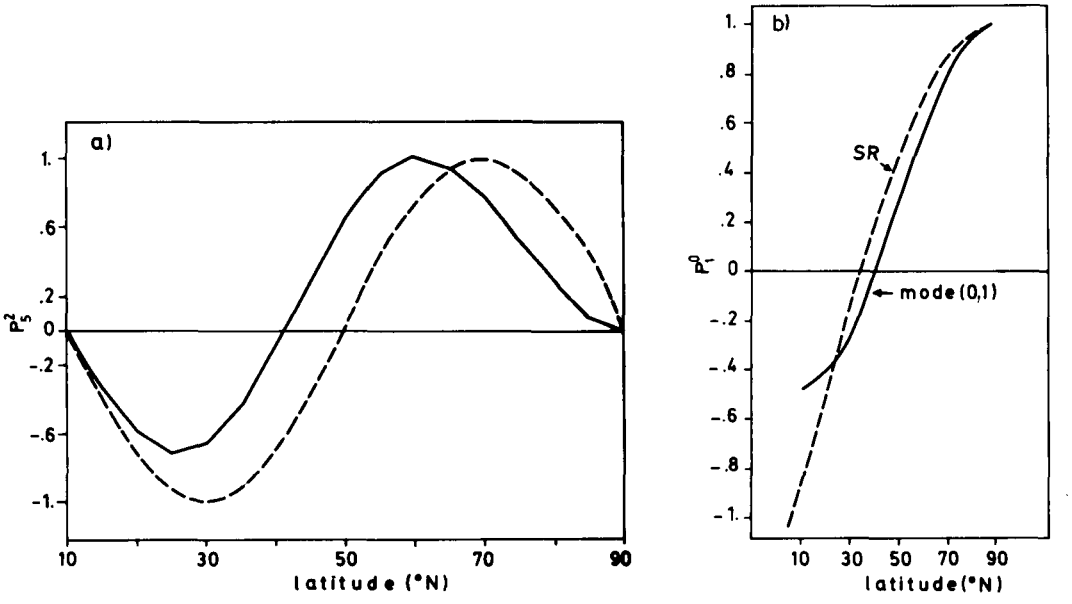

Fig. 1. (a) Solid: second discrete eigenmode ($\tilde{n} = 2$) of the Laplacian for $m = 2$ (see Subsection 1.3). Dashed: second eigenfunction of the Laplacian on the β-plane. (b) Solid: first non-constant discrete eigenmode ($\tilde{n} = 1$) of the Laplacian for $m = 0$ (line is drawn for optical orientation only). Dashed (labelled by SR): super-rotational mode ($\sin\phi$), normalized the same way as the discrete eigenmode.

$$P_n^m(\phi_0) = P_n^m(\phi_e) = 0, \quad \text{for } m \neq 0, \tag{9b}$$

$$\partial_\phi^B P_n^0(\phi_0) = \partial_\phi^B P_n^0(\phi_e) = 0, \quad \text{for } m = 0, \tag{9c}$$

and computed numerically on our data grid. Here ∂_ϕ^B denotes an appropriate difference approximation of the ϕ-derivative at the channel boundaries. We introduce the relation

$$n = |m| + 2\tilde{n} - 1, \tag{9d}$$

with $\tilde{n}$ denoting the number of nodes between ϕ_0 and ϕ_e minus one. For further details refer to Appendix B. Two important examples of meridional eigenmodes are given in Fig. 1.

3. BO definition and case selection

3.1. Definition

We eliminate long term trends and seasonal variability by transforming our time series M_m with

$$N'_m = M'_m/\sigma_m, \tag{10}$$

where the $M'_m = M_m - \langle M_m \rangle$ are deviations from long-term monthly means $\langle M_m \rangle$. The transform (10) shifts the mean into zero and the normalization with $\sigma_m = \sqrt{\langle (M'_m)^2 \rangle}$ leads to unit variance. Here we discuss $M_m = C(A_z A_m)$ and its persistent large excursions $N'_m \geqslant 1$ from normal. After S88, the definition of a BO period related to m is:

the basic period of BO consists of at least $P_0 = 3$ consecutive days with $N'_m \geqslant N_0 = 1$; (11a)

in addition, preceding or following days with $N'_m \geqslant 0.75\, N_0$ belong to the BO period; (11b)

if there are preceding or following days with $N'_m \geqslant N_0$ being separated from the BO period after (11a) and (11b), they are added to the BO period, provided that the separation period consists of 3 days with $N'_m > 0.20\, N_0$ at most; the separation days belong to the BO period too. (11c)

The definition depends on two threshold parameters and its sensitivity to changes in N_0, P_0 was discussed in S88. Here, it is important that BO's after (11) represent extreme energy states of the atmosphere.

3.2. Prerequisites for adopting a composite technique

For $m = 2$, we count 73 BO cases during 1967–1976, defined by (11). It is neither possible to discuss and exhibit the energetics of each single case, nor feasible to average over all cases. Since composite energetics is an alternative, we have to be careful in grouping the events according to their main characteristics. Case selection is done in 5 steps.

(i) The frequencies of durations of $m = 2$ BO's, as given in S88 (Fig. 5), indicate several very persistent BO's. Indeed, about 30% of them persist longer than 7 days. Consequently, one can expect a drastic transformation of the flow induced by the amplification of zonal wave $m = 2$. We therefore restrict our interest to ultrapersistent cases with a duration of more than 7 days (but less than 15 days).

(ii) We selected winter cases only (October–February). In Table 1, we have listed all of the $m = 2$ BO cases consistent with (i) and (ii). Fortunately, it appears that the standard deviation of durations is less than 15% of the mean duration value (10.8 days). This is an important prerequisite for constructing composite averages.

(iii) Each single conversion stands for the potential of the underlying process to amplify the wave. However, only the excess or effective conversion is relevant, since it is not balanced by other terms. As before, we focus on $C(A_z A_2)$ as part of the available potential energy budget

$$\partial A_2/\partial t = C(A_z A_2) - C(A_2 K_2) + \text{other terms}.$$

We have to assure that the very large conversion $C(A_z A_2)$ indeed drives A_2 to a great extent. At the same time, this term has to feed $C(A_2 K_2)$ in order to provide an efficient baroclinic input for K_2. The efficiency of these actions is measured by the time mean of (not normalized after (10))

$$R_0 = \{\partial A_2/\partial t + C(A_2 K_2)\}/C(A_z A_2) \tag{12}$$

for single cases. If $0 < R_0 \ll 1$, $C(A_z A_2)$ is large but the sum of the other terms is even larger. In this case, processes different from baroclinic input dictate the development of A_2. For the BO's, selected after (i) and (ii), the average action of $C(A_z A_2)$ as measured by R_0 is shown in Fig. 2.

(iv) In order to assure that during our BO events strong baroclinic activity occurs, we have

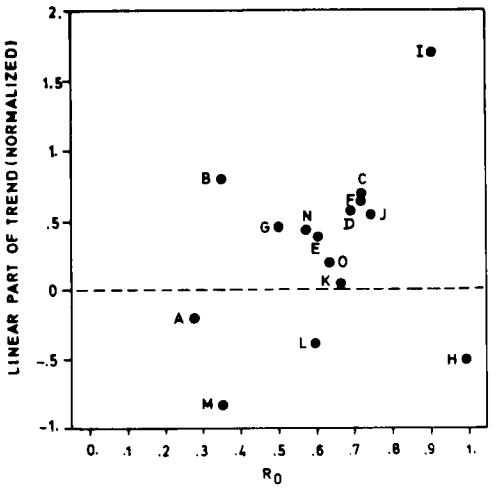

Fig. 2. $R_0 - Q_0$ characteristics of super-persistent $m = 2$ winter BO cases. For definitions see text.

to show that $C(A_2 K_2)$ is then well above normal. This characteristic is defined by the time average of

$$W_0 = \{C(A_2 K_2) - \langle C(A_2 K_2)\rangle_j\}/\sigma_j, \tag{13}$$

where $\langle\ \rangle_j$ denotes a long-term mean of month j and σ_j stands for the long-term standard deviation of $C(A_2 K_2)$, respectively. Due to the bad quality of ω-estimates, this parameter does not satisfactorily indicate baroclinic activity under normal conditions. However, as indicated in S88, it will perform better during BO events. In fact, in most of our ultra-persistent winter cases, W_0 is well above normal (Tables 1, 2).

In order to be sure that this is indicative of amplification, we fit single normalized $K_2(t)$ evolutions to a quadratic trend

$$a_0 + a_1 t + a_2 t^2 \rightarrow Q_0 = a_1. \tag{14}$$

A positive linear coefficient a_1 is a direct measure for systematic amplification of K_2 during an outbreak event. By inspecting Fig. 2, we find only a few cases in which a_1 by being negative does not meet our requirements. Cases A, H, L, M of Table 1 have therefore been discarded from this point on.

(v) In the Introduction, we have supposed that there are supplementary processes (7), (8) favourable for the BO dynamics. It is tempting to split up the ensemble of cases into two subclasses: For the first one (G_0), no considerable input due to nonlinear interaction terms $BTPLL_2$ or $BTPLS_2$ [viz. eqs. (7), (8)] is observable, in contrast to the situation found for the second subclass (G_+). To this end, $BTPLL_2$ and $BTPLS_2$ were normalized after (10) and then time-averaged over single events (see Table 1). Whenever at least one of these averages is well above

Table 1. *Winter baroclinic outbreak cases for $m = 2$ with duration longer than 7 days (and shorter than 15 days). They are grouped with respect to possible subsidiary processes favourable for driving the event (for further details see text)*

Case label	Event from–to	Duration	Group	*BTPLL*	*BTPLS*	W_0
A	12–21 Feb. 1967	10	discarded	−0.031	−0.516	0.212
B	30 Jan.–8 Feb. 1972	10	G_0	0.260	−0.332	0.906
C	22 Jan.–3 Feb. 1975	13	G_+	0.842	−0.025	0.804
D	2–13 Jan. 1971	12	G_0	0.015	−0.335	0.250
E	2–15 Dec. 1972	14	G_+	0.924	0.208	1.385
F	3–12 Nov. 1976	10	G_+	0.555	0.708	1.494
G	2–12 Dec. 1976	11	G_+	0.583	0.368	1.096
H	3–13 Nov. 1967	11	discarded	0.037	0.536	0.687
I	24–31 Oct. 1970	8	G_+	0.553	0.253	1.644
J	16–26 Oct. 1976	11	G_+	0.206	1.343	1.847
K	3–14 Jan. 1974	12	G_0	−1.548	−0.141	1.646
L	26 Feb.–7 Mar. 1967	10	discarded	0.576	−0.342	1.409
M	9–17 Jan. 1969	9	discarded	−0.329	−0.589	0.443
N	4–13 Feb. 1974	10	G_0	0.162	−0.342	1.915
O	17–24 Dec. 1974	8	G_0	−0.112	−0.335	0.926

Table 2. *Case averaged activity parameters W_0 after (13), R_0 after (12), Q_0 after (14) and K_2/K_{total} for two subensembles G_0, G_+ (definitions see text); the values are normalized after (10) except for R_0*

Parameter	W_0	R_0	Q_0	K_2/K_{total}	W_0 (BO I)
G_+ (6 cases)					
average	1.38	0.70	0.74	1.48	1.53
standard deviation	0.38	0.13	0.49	0.68	0.53
G_0 (5 cases)					
average	1.12	0.59	0.41	1.27	0.94
standard deviation	0.68	0.14	0.31	0.52	0.42
t-parameter threshold (90%)	0.58	0.98	0.94	0.41	1.48

zero, we put that case into group G_+, otherwise into group G_0.

We test the hypothesis that baroclinic activity is larger for G_+ than G_0. For comparison sake, we select some parameters of activity: W_0 after (13), R_0 after (12), Q_0 after (14) and the fractional kinetic energy K_2/K_{total}. The differences between G_0 and G_+ were tested using a one-tailed *t*-test with 9 effective degrees of freedom and 10% error probability (Table 2).

Significant differences on that level were not found, yet the activity parameters for G_+ are a bit larger than the other ones. This testing may not be specific enough because averages over a whole BO-period can mask differences at the amplification stage. Therefore, another test was made utilizing averages over the first half of the events (BO I), showing that no significant difference can be detected on the 90% level except for W_0. This single significant result does not justify the splitting of the BO ensemble into G_0, G_+ subclasses.

4. Composite energetics for $m = 2$ outbreak events

4.1. Two-dimensional spectral kinetic energy evolution

BO dynamics are highly non-stationary and composite averages are only meaningful for short sub-periods. They are defined as: (i) BO − 5: the 5 days before the onset of BO. (ii) BO I: the first half of the BO event (approximately 5 days). (iii) BO II: the second half of the BO event (approximately 5 days). In cases having an odd number of days, BO I and BO II overlaps for one day. (iv) BO + 5: the 5 days following the BO episode. Figs. 3a–d display the respective case- and period-averages for the two-dimensional spectral kinetic energy at 500 mb. Note that all values are normalized after (10). The averages were tested against the null-hypothesis that they are zero, being normal (univariate two-tailed *t*-test with 10% error probability). Averages are displayed in Figs. 3a–d if statistically significant at a 90% level. The isolines serve for optical orientation only.

A drastic reorganization of kinetic energy during BO-events is to be seen. This is the most interesting result of this section. Beginning with BO − 5 (Fig. 3a), we note that only two spectral regions appear to be well above normal. They are situated in the vicinity of ($m = 5$, $\tilde{n} = 1$) and ($m = 1$, $\tilde{n} = 4$). Recall the fact that $\tilde{n}$ counts the nodes (minus one) of the meridional wavy structure. Both kinetic energy centers completely lose their character during the course of the BO events.

During the first half of the episodes (BO I; Fig. 3b), a new regime has been established. Of course, $m = 2$ has achieved the predominant role in the spectrum. Surprisingly, there are only two meridional components of $m = 2$ which profit from the gain of energy: $\tilde{n} = 2$ and $\tilde{n} = 4$ (the latter playing no further role). A zonal mean flow component ($\tilde{n} = 4$) showing above normal amplitude indicates that the meridional structure of u in 500 mb is finer than normally observed. Also, this feature is no longer present at later stages of BO development. Nearly as important as the amplification of only a few spectral eddy components is the below-normal spectral energy content in vast regions of the spectrum. This enforces the impression that the spectrum is transforming into an unusually simple pattern during the first stage of development. The picture drawn for BO I is even more drastic for BO II.

Now, the kinetic energy is accumulated in only two spectral components of $m = 2$ with absolute predominance of ($m = 2$, $\tilde{n} = 2$) (cf. Fig. 1a). The rest of the spectrum is either at a normal or significantly below-normal level. This situation is ideal for constructing low-order models of quasi-geostrophic dynamics. Indeed, a value as high as

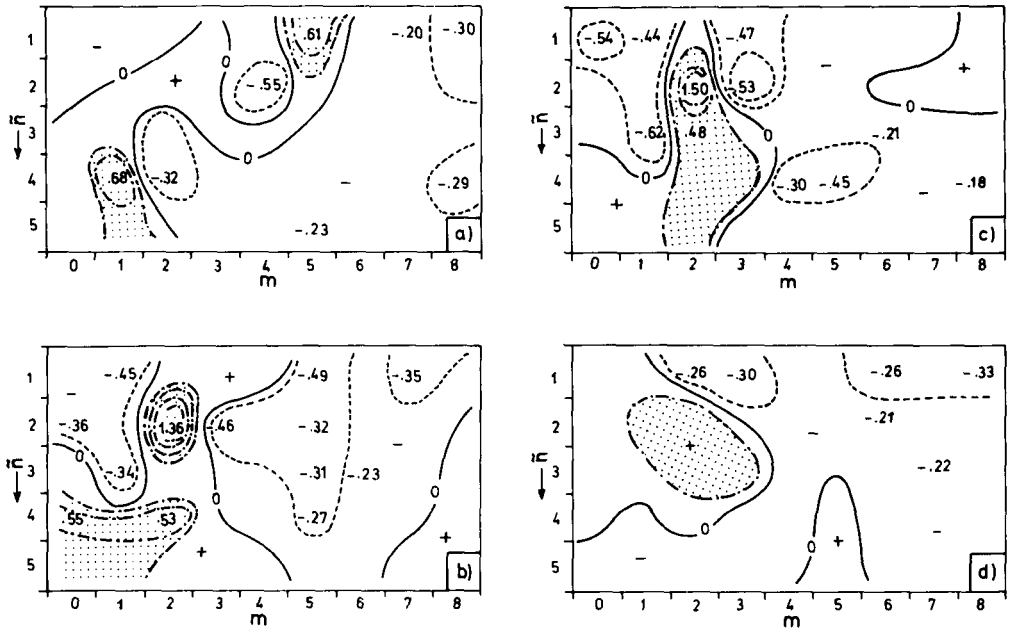

Fig. 3. Two-dimensional spectral distribution of kinetic energy in 500 mb. Averages over the combined ensembles G_+ and G_0 are given if statistically significant on a 90% level. Isolines are for optical orientation only.
(a) Average over 5 days before onset of BO's (BO − 5).
(b) Same as (a), except for period BO I.
(c) Same as (a), except for period BO II.
(d) Same as (a), except for averages over 5 days after the end of BO's (BO + 5).

1.50 for ($m = 2$, $\tilde{n} = 2$) marks a substantial energy accumulation since average and standard deviation of ($m = 2$, $\tilde{n} = 2$) are the largest in the eddy spectrum from the beginning. This value means that ($m = 2$, $\tilde{n} = 2$) contains about 10% of the total kinetic energy at 500 mb (about 20% of eddy kinetic energy) on average! In single BO cases, this figure amounts to 25% of eddy kinetic energy. Again, this distribution is extraordinary. Note, that Figs. 3a–d only representing case-averaged distributions, somewhat simplify the situation in single events, which may show a more complicated spectral structure. Nevertheless, our results indicate that amplified spectral components with $m \neq 2$ are not truly characteristic of BO events. Therefore, it seems proper to adopt a low-order model, if the simulation of the above mentioned evolution is intended for subsequent work. During BO II we find that $\tilde{n} = 1$ of the zonal mean flow exhibits substantially less energy than normal. This result is confirmed by the fact that it is this spectral component which contributes most of the zonal mean APE during maximum baroclinic activity of $m = 2$ (not shown). The meridional structure of ($m = 0$, $\tilde{n} = 1$) is given by Fig. 1b, revealing that this component is more or less representative for the super-rotational mode of $m = 0$ in the picture of Legendre polynomials.

We end with BO + 5 (Fig. 3d). The overall impression is that the energy distribution of BO II has been conserved, although on a less spectacular level. This finding indicates that the dramatic drop of K_2 at the end of a BO example given in S88 (Fig. 2) is not representative of the normal development of this parameter. Note that the synoptic scale waves have not yet reached their usual energy level despite the fact that their baroclinic activity has then switched to above-normal values (cf. Fig. 3d).

4.2. Two-dimensional spectral energy conversion evolution

Next, we are interested in the development of two-dimensional decomposed and normalized $C(A_z A_{m\hat{n}})$ which, of course, drives the BO dynamics. As before, we consider $C(A_z A_{m\hat{n}})$ as a reliable indicator of the baroclinic activity of wave modes. Therefore, we present the results on these conversions first, adopting the methodology of the previous section. Subsequently, we will show that the other baroclinic conversion, $C(A_{m\hat{n}} K_{m\hat{n}})$, displayed very similar spectral structural changes.

We begin with the average over BO − 5 (Fig. 4a), noting an activity center for shorter scales ($m = 4, 5$). This situation is similar to that derived theoretically from GCM-results (cf. Gall et al., 1979a, b). Ultralong waves as well as the so-called synoptic waves exhibit a somewhat below-normal activity at this stage.

The BO I phase (Fig. 4b) shows a dramatic change in the centers of baroclinic activity. Now, $m = 2$ has taken over all of the relevant baroclinic activity which is in good agreement with Fig. 3b. Quite a few waves with $m \neq 2$ operate at a normal level of baroclinic activity, however. On the other hand, the large valued baroclinic conversion for $m = 2$ is substantial even in the non-normalized terms since it is known (cf. S88) that $m = 2$ is predominant in winter with respect to the conversion $C(A_z A_m)$.

As can be expected from Fig. 3c, the situation is even simpler during BO II (Fig. 4c). Now the baroclinic activity of waves $m \neq 2$ is significantly below normal values. Clearly, $m = 2$ has taken over the dominant role in releasing energy from the zonal mean state. Correspondingly, a low-order model would fit the two-dimensional spectral structure of the baroclinic input conversion quite well.

After the phase of dramatic BO development, baroclinic activity tends to decline back to normal conditions (cf. Fig. 4d, for BO + 5). However, $m = 2$ turns to below-normal baroclinic activity as can be expected from our definition (11).

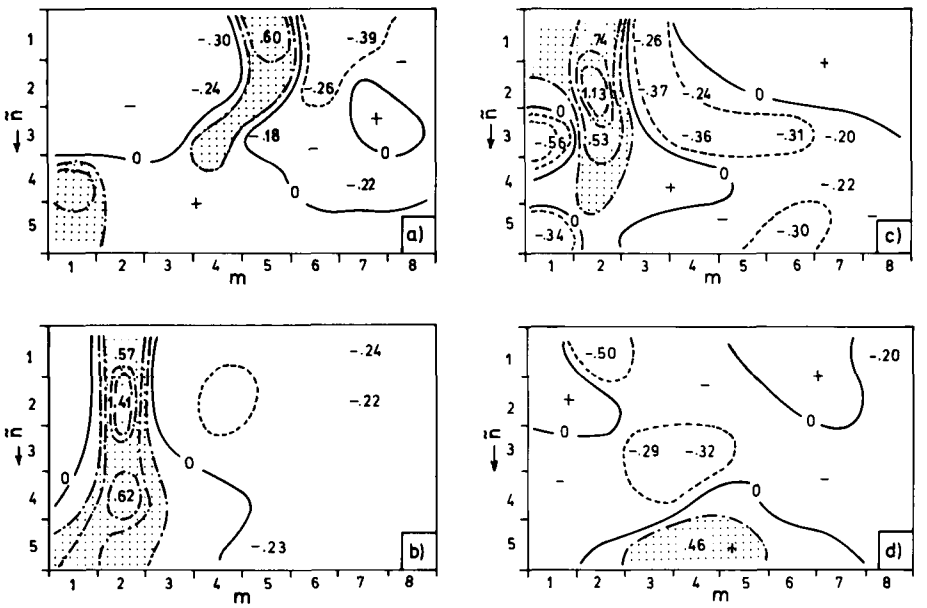

Fig. 4. Two-dimensional spectral distribution of conversion $C(A_z A_{m\hat{n}})$. Averages over the combined ensembles G_+ and G_0. Plotting conventions as in Figs. 3a–d.

(a) Average over 5 days before onset of BO's (BO − 5).

(b) Same as (a), except for period BO I.

(c) Same as (a), except for period BO II.

(d) Same as (a), except for period BO + 5.

For the sake of completeness we exhibit the BO results for $C(A_{m\tilde{n}}K_{m\tilde{n}})$ too. First, Fig. 5a demonstrates the drastic enhancement of that $m=2$ energy conversion during BO I. It appears that $C(A_{22}K_{22})$ follows the development of $C(A_z A_{22})$ very closely. Comparing the ($m=2$, $\tilde{n}=2$) value with all others, we find that this leading mode dominates also this conversion spectrum. During the second half of the events (BO II, Fig. 5b), we encounter the strongest conversion in the $C(A_{22}K_{22})$ term, but now other meridional modes (e.g., $\tilde{n}=1$) are strongly affected too.

4.3. *Statistical test of some a-priori hypotheses on BO dynamics*

Subsections 4.1 and 4.2 reveal some BO characteristics on an *a posteriori* basis. On the other hand, we can formulate certain *a priori* hypotheses, by postulating enhanced levels of kinetic energy K_2 and $C(A_2K_2)$ conversions of the BO wave $m=2$. Moreover, in S88, it was speculated that kinetic energy as well as baroclinic activity of shorter waves ($m=5$–8, say) would be suppressed a bit. Therefore, an additional effort is made to test our *a priori* hypotheses as well as selected *a posteriori* findings independently by (i) the parametric t-test and (ii) by two non-parametric tests T_1, T_2, similar to those introduced by von Storch (1985) into the meteorological literature.

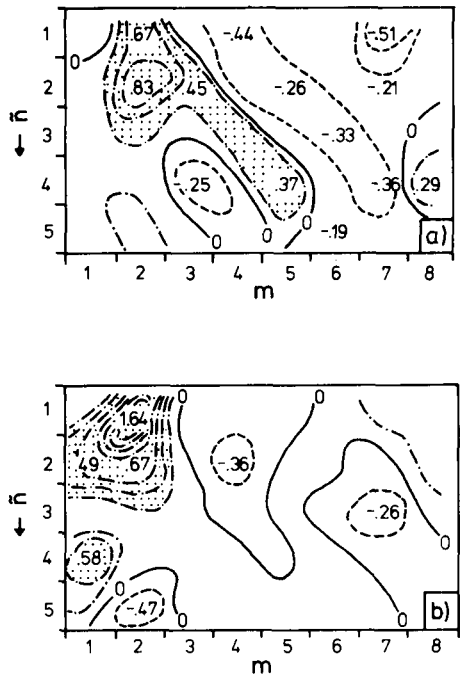

Fig. 5. Two-dimensional spectral distribution of conversion $C(A_{m\tilde{n}}K_{m\tilde{n}})$. Averages over the combined ensembles G_+ and G_0. Plotting conventions as in Figs. 3a–d.
(a) Average over period BO I.
(b) Average over period BO II.

To be more precise, we are dealing with the former $m=2$ BO case ensemble (11 cases) for BO − 5, BO I, BO II, BO + 5 respectively. Accordingly each test parameter is an average over 5 days or nearly so. A comparison is made with 28 averages (each for 5 successive days) drawn independently by chance out of BO-free winter periods 1967–1976. The test statistic T_1 is chosen to be (R_{0p} is the pth averaged parameter for the BO-ensemble, R_p the same except for the comparison ensemble):

$$T_1(0)=\sum_{p=1}^{11}(R_{0p}-R_p),$$

where the choice of the 11 R_p averages is by chance. Therefore, $T_1(0)$ is not unique but distributed around an ensemble averaged T_1. Note that our tests are one-sided, since definite hypotheses are tested. The statistic T_2 is based on rank testing. To this end combine all (R_0, R) into a single ensemble and bring them in increasing order. The resulting counting index of R_{0p} is N_{0p}, that of R_p is N_p. Then

$$T_2(0)=\sum_{p=1}^{11}\left(N_{0p}-\begin{matrix}\text{expectation of counting}\\ \text{index}\end{matrix}\right).$$

The non-parametric nature of T_1, T_2 under the null hypothesis that R_0 and R belong to the same ensemble is guaranteed by arbitrarily mixing up the R_{0p} and R_p, or N_{0p} and N_p, combined into one ensemble. This is done 100 times and $T_1(q)$, $T_2(q)$ are recomputed afterwards (q denoting the single mixing event). This procedure yields a frequency distribution of $T_1(q)$ and $T_2(q)$, which is the basis of the test.

Provided that the BO ensemble is nothing else but a subensemble of the BO-free ensemble (null hypothesis H_0), the range limits $T_1(q,\alpha)$, $T_2(q,\alpha)$

are exceeded by a fraction α of $T_2(q)$ or $T_2(q)$ values; α denotes the error probability for rejecting the null hypothesis. Here, we choose $\alpha = 0.05$. The standard t-test for average differences completes the testing program; its layout is the same as for T_1, T_2. Note that each parameter R is tested separately.

The following *a priori* parameters:

$C(A_2 K_2)$, K_2 (500 mb), K_{5-8} (500 mb),

$$\sum_{m=5}^{8} C(A_m K_m), \quad \sum_{m=5}^{8} C(A_z A_m)$$

as well as the *a posteriori* parameters $C(A_{22} K_{22})$, K_{22} (500 mb), K_{22} (500 mb)/K_2 (500 mb) are tested. The results are collected in Table 3. No entry of cases was made, if the null-hypothesis cannot be rejected. Entries without brackets were made if at least two tests lead to the rejection of the null hypothesis. Bracketed entries indicate that only one test suggests the rejection but others do not. The respective tests leading to the rejection of H_0 are given in Table 3, too. Here a few words about the deficiencies of T_1, T_2 (as noted by von Storch, 1985) are in order.

It turns out that T_1, T_2 are sensitive to significant variance differences between the two ensembles R_0, R. Indeed, non-parametric tests tend to be more sensitive to differences in frequency distribution characteristics than to average differences. Therefore, another entry in Table 3 is the notation V for significant variance differences on a 95% level as revealed by an F-test. On the other hand, the ordinary t-test is approximately unaffected by variance differences. Therefore the rejection of the null-hypothesis by the t-test (denoted by entry t) as well as by either T_1 or T_2, may indicate that variance deviations did not cause the rejection by T_1 or T_2.

Table 3. *Test results on various parameters of BO activity as compared to BO-free periods (details see text); entries denote rejection of null hypothesis H_0 with 5% error probability (one-tailed testing)*

(a) *A priori* hypotheses

Period	$C(A_2 K_2)$	K_2	K_{5-8}	$\sum_{m=5}^{8} C(A_m K_m)$	$\sum_{m=5}^{8} C(A_z A_m)$
BO − 5					
BO I	1.26 >normal T_1, t	1.24 >normal T_1, T_2, t/V	−0.51 <normal T_1, T_2, t	(−0.43) (<normal) t	−0.20 <normal T_2, t
BO II	1.29 >normal T_1, T_2, t	1.56 >normal T_1, T_2, t/V			
BO + 5		0.45 >normal T_1, t			

(b) *A posteriori* hypotheses

Period	K_{22}	$C(A_{22} K_{22})$	K_{22}/K_2
BO I	1.36 >normal T_1, T_2, t/V	(0.83) (>normal) t	(0.69) (>normal) t
BO II	1.50 >normal T_1, T_2, t/V		0.69 >normal T_1, t
BO + 5	0.40 >normal T_1, T_2		

We begin with the *a priori* hypotheses (Table 3). It can be seen that the above-normal development of $C(A_2 K_2)$ and K_2 during long-lasting winter $m = 2$ BO's is statistically significant. Out of the other parameters the suppression of energy and baroclinic input related to smaller scales can be accepted with similar confidence but for the BO I phase only. Suppression of $\sum_{m=5}^{8} C(A_m K_m)$ is indicated by a single test for BO I and we refer to it with minor confidence only.

Next, we turn to the *a posteriori* hypotheses. Here, we can accept the predominance of kinetic energy of ($m = 2$, $\tilde{n} = 2$), as indicated by Fig. 3b, c. The same can be stated for the fraction of kinetic energy of ($m = 2$, $\tilde{n} = 2$) related to the $m = 2$ kinetic energy. We face a different situation as to energy conversion $C(A_{22} K_{22})$. Here, we are able to reject the normal conditions hypothesis by t-testing only (normal is denoted by zero).

5. Conclusions

We have studied a number of persistent states of northern hemisphere middle latitude circulation with vigorous above-normal baroclinic activity of the single wave $m = 2$. Despite the fact that these episodes are relatively rare, they provide examples of outstanding dynamics. In fact, persistent episodes with vigorous above-normal baroclinic input $C(A_z A_2)$ develop like a baroclinic outbreak (BO), characterized by a likewise strong enhancement of the second baroclinic conversions, $C(A_2 K_2)$, and kinetic energy, K_2. Our definition of the above-mentioned amplification events is more specific than those given by Itoh (1983), Hansen (1986) or Tsay and Kao (1978a, b), since these authors collect nearly all amplification episodes of one zonal wave (or wavegroup) within a given time. Here we further restrict the sample by demanding a certain single energy conversion to be unusually large for a longer time span. Whereas previous studies on amplification episodes were not able to discern a leading mechanism by statistical means, our relatively homogeneous set of events enables us to check the hypotheses of the Introduction by using simple testing routines. The main results are as follows.

(i) The *a priori* hypotheses that kinetic energy K_2 and conversion $C(A_2 K_2)$ are strongly enhanced, parallel to the abnormal evolution of $C(A_z A_2)$, is confirmed.

(ii) We found that the two-dimensional spectral distribution of kinetic energy at 500 mb and of hemispherically averaged conversion $C(A_z A_{m\tilde{n}})$ are strongly distorted during ultrapersistent winter BO's for $m = 2$. There are only few spectral components which profit from the strong baroclinic injection coming from the zonal mean available potential energy. It is the mode ($m = 2$, $\tilde{n} = 2$) which shows spectacular amplification on average. The kinetic energy of ($m = 2$, $\tilde{n} = 2$) is significantly enhanced towards above-normal (*a posteriori*).

(iii) The respective driving by $C(A_{22} K_{22})$ is above-normal, but the significance of this result is not without doubt.

(iv) The suppression of smaller scales ($m = 5$–8) during $m = 2$ BO-events is manifested by below-normal kinetic energy and baroclinic input $A_z \rightarrow A_{5-8}$ at earlier stages of the process. Other statements in this direction cannot be confirmed by our test procedure.

We have studied only one small subset of the ensemble of $m = 2$ amplification events, leaving other subsets for further investigation. The significance of our results is obvious despite the smallness of our subset: from this fact it cannot be concluded that the specific pattern of wave $m = 2$ activity, displayed here, is exotic and irrelevant. On the contrary, this prototype of wave activity plays a role in the everyday dynamics of the wave. It cannot always be observed in pure form since other prototypes (e.g., barotropic instability, nonlinear wave–wave interactions) may additionally exist and operate together to form the observed atmospheric dynamics. Therefore, it is worthwhile to discern the mechanisms of these prototypes one after another before investigating their cooperation or competition. It is, moreover, obvious from the observed large amplitudes, pronounced transience and spectacular evolution that we are dealing with highly nonlinear dynamics. Whereas the theoretical understanding of the atmospheric flow near equilibrium (e.g., maintenance of blockings, signals from abnormal low-frequency forcing) is well developed, the theoretical explanation of observed nonlinear excursions far from equilibrium is still lacking.

6. Appendix A

List of symbols not explained in the text

$\langle\ \rangle$	time mean
A_z	$(p_B/g\sigma_0)[\frac{1}{2}\{\partial(\overline{\Phi} - [\Phi]_{\phi_1}^{\phi_2})/\partial p\}^2]_{\phi_1}^{\phi_2}$
A_m	$(p_B/g\sigma_0)[\frac{1}{2}\{\partial\Phi_m/\partial p\}^2]_{\phi_1}^{\phi_2}$
$J(X, Y)\|_m$	Jacobian of X, Y projected onto wave m
λ, ϕ, t	longitude, latitude, time
ϕ_A, ϕ_B	boundaries of meridional averaging
f_0	Coriolis parameter for $\phi = 45°$ N
ρ, α	density, specific volume of dry air
p, θ	pressure, potential temperature
R	gas constant (dry air)
c_p, c_v	specific heat at constant pressure, constant volume
p_B	1000 mb pressure
Φ, Ψ	geopotential, streamfunction
ω	dp/dt
a_m, b_m	zonal Fourier-coefficients of the field Z related to zonal wavenumber m
$\overline{X}$, X'	zonal mean of X, deviation from $\overline{X}$
X_m	field X projected onto zonal wavenumber m
$X_{m\tilde{n}}$	field X restricted to zonal wave m and meridional mode $\tilde{n}$
$K_{m\tilde{n}}$	globally averaged kinetic energy of zonal wave m restricted to normal mode $\tilde{n}$
Δp_i	pressure increments ($\Delta p_1 = 200$ mb, $\Delta p_2 = 500$ mb) for baroclinic expressions and ($\Delta p_1 = 400$ mb, $\Delta p_2 = 400$ mb, $\Delta p_3 = 200$ mb) for barotropic expressions
a	earth radius
g	earth gravity constant

6. Appendix B

Meridional eigen-structures

We solve the eigenproblems given by (9a, b, c).

Let $z_m = a_m - ib_m$ be a complex version of a zonal Fourier coefficient of the field Z, depending on the latitude ϕ [see S88]. The matrix ∇^2 is the discretized Laplacian ∇^2 for a channel $10°\text{N} \leqslant \phi \leqslant 90°\text{N}$ on the sphere. The gridded values of z_m form a vector $\boldsymbol{z}$. The matrix ∇^2 and $\boldsymbol{z}$ are related to an equidistant grid $\phi_0 = 10°\text{N} \leqslant \phi_i \leqslant \phi_e = 90°\text{N}$ with $i = 0, \ldots 16$. This special eigenmode structure is consistent with the given data structure and the fact that our quasi-geostrophic evaluation model is not valid in the tropics south of 15° N, say.

Then we expand z_m into the eigenmodes of the ϕ-discrete version ∇^2 of the Laplacian:

$$\nabla^2 = (a\cos\phi)^{-1}\{\partial(\cos\phi\,\partial/\partial\phi)/\partial\phi\} + (a\cos\phi)^{-2}\,\partial^2/\partial\lambda^2,$$

adopting spherical geometry with lateral channel boundaries. A typical element of ∇^2 is

$$\frac{1}{\cos\phi_i(\Delta\phi)^2}\{\delta_{i-1,j}\cos(\phi_i + \Delta\phi/2) + \delta_{i+1,j}\cos(\phi_i - \Delta\phi/2) - \delta_{i,j}(\cos(\phi_i + \Delta\phi/2) + \cos(\phi_i - \Delta\phi/2) - m^2/\cos\phi_i)\}, \quad \text{(B1)}$$

if ∂_ϕ is chosen to be a central difference approximation. The Kronecker symbol $\delta_{i,j}$ has its usual meaning.

For ∂_ϕ^B we use:

$$\partial_\phi^B P_n^0(\phi_0) = (P_n^0(\phi_1) - P_n^0(\phi_0 - \Delta\phi))/(2\Delta\phi), \quad \text{(B2a)}$$

$$\partial_\phi^B P_n^0(\phi_e) = (P_n^0(\phi_e + \Delta\phi) - P_n^0(\phi_e - \Delta\phi))/(2\Delta\phi). \quad \text{(B2b)}$$

The polar condition (B2b) should be defined more refined, but the meridional eigenstructure is only slightly affected by this refinement.

The eigensolutions are eigenvectors $\boldsymbol{P}$ on the equidistant data-grid being orthogonal with weight $\cos\phi$. The modal decomposition of $\boldsymbol{z}$ is exact in the sense that a finite number of eigenvectors $\boldsymbol{P}_m^k(\phi_i)$ suffices to represent exactly the observed meridional structure of a_m, b_m for each m at all grid points given. Moreover, using usual vector algebra and Φ-data north of 10° N we note that the familiar linear balance equation (1) show no singular behavior due to zero $f = f(90°\text{N})\sin\phi$ at the equator. Indeed we circumvent the familiar balancing problem for Legendre polynomials as described by Merilees (1968) and others. For more details on the balancing between Φ and Ψ, see Egger and Schilling (1983).

Another problem arises from the evaluation of the Jacobian $J(X, Y)$ projected onto one interacting triad of modes under the constraints of conserving energy and enstrophy. This problem is solved by constructing a special discretization of terms like $\boldsymbol{P}_k\,\partial\boldsymbol{P}_j/\partial\phi$. This method was reported in Egger and Schilling (1983).

REFERENCES

Egger, J. and Schilling, H.-D. 1983. On the theory of the long-term variability of the atmosphere. *J. Atmos. Sci. 40*, 1073–1085.

Egger, J., Metz, W. and Müller, G. 1986. Forcing of planetary-scale blocking anticyclones by synoptic-scale eddies. *Advances of Geophysics*, Vol. 29 (eds. R. Benzi, B. Saltzman and A. Wiin-Nielsen). Orlando: Academic Press, 183–197.

Fischer, G. 1984. Spectral energetics analysis of blocking events in a general circulation model. *Contrib. Atm. Phys. 57*, 183–200.

Gall, R., Blakeslee, R. and Somerville, R. C. 1979a. Baroclinic instability and the selection of the zonal scale of the transient eddies of middle latitudes. *J. Atmos. Sci. 36*, 767–784.

Gall, R., Blakeslee, R. and Somerville, R. C. 1979b. Cyclone scale forcing of ultralong waves. *J. Atmos. Sci. 36*, 1692–1698.

Hansen, A. R. 1986. Observational characteristics of atmospheric planetary waves with bimodal amplitude distribution. *Advances of Geophysics*, Vol. 29 (eds. R. Benzi, B. Saltzman, A. Wiin-Nielsen). Orlando: Academic Press, 101–133.

Hansen, A. R. and Chen, T. C. 1982. A spectral energetics analysis of atmospheric blocking. *Mon. Wea. Rev. 110*, 1146–1165.

Hansen, A. R. and Sutera, A. 1984. A comparison of the spectral energy and enstrophy budgets of blocking versus nonblocking periods. *Tellus 36A*, 52–63.

Itoh, H. 1983. An observational study on the amplification of planetary waves in the troposphere. *J. Met. Soc. Japan 61*, 568–589.

Kung, E. C. and Masters, S. E. 1983. Large scale energy transformations in the high latitudes of the northern hemisphere. *J. Atmos. Sci. 40*, 1061–1072.

Merilees, P. E. 1968. On the linear balance equation in terms of spherical harmonics. *Tellus 20*, 200–202.

Schilling, H.-D. 1986. On atmospheric blocking types and blocking numbers. *Advances of Geophysics*, Vol. 29 (eds. R. Benzi, B. Saltzman, A. Wiin-Nielsen). Orlando: Academic Press, 71–99.

Schilling, H.-D. 1987. Observed baroclinic energy conversions in wavenumber domain for 3 winters: A time series analysis. *Mon. Wea. Rev. 115*, 520–538.

Schilling, H.-D. 1988. Baroclinic outbreak episodes in wavenumber domain. *Tellus 40A*, 188–204.

Tsay, C.-Y. and Kao, S.-K. 1978a. Linear and nonlinear contributions to the growth and decay of the large-scale atmospheric waves and jet stream. *Tellus 30*, 1–14.

Tsay, C.-Y. and Kao, S.-K. 1978b. Contributions to the growth and decay of large-scale eddy available potential energy. *Tellus 30*, 383–391.

Von Storch, H. 1985. *Über die Verifikation atmosphärischer Zirkulationsexperimente*. Habilitationsschrift, Universität Hamburg, Meteorological Institute, Bundesstr. 55, D2000 Hamburg 13, FR Germany (available from von Storch upon request).